:brass, S. E. & Taylor, R. N. (1997). *Géotechnique* 47, No. 2, 235–253

The development and evaluation of a constitutive model for the prediction of ground movements in overconsolidated clay

S. E. STALLEBRASS* and R. N. TAYLOR*

stress–strain response of overconsolidated depends both on its current state and on loading history followed to reach that state, particular the relative directions of the rent and previous loading paths. A constitu- soil model is developed which predicts this aviour by allowing elasto-plastic deforma- s controlled by two nested kinematic hard- ıg surfaces inside a conventional Modified n-clay state boundary surface. This relatively ightforward model requires only eight para- ers, each with a rational basis, and which be determined from a small number of well- trolled stress path tests. Predictions of soil aviour using this model are compared with ı from triaxial stress path tests. The close ement confirms that the essential features of behaviour are predicted by the model. The er implications of the use of the model in echnical analysis are illustrated by compar- predictions made using the model (in unction with finite element analysis) with ı from a specially commissioned series of rifuge tests of a circular foundation loaded overconsolidated clay. The stress history of soil was carefully controlled in the experi- ts and was replicated in the course of the yses. The computations reproduced the n characteristics of the observed ground ement, in particular the surface profile. In rast, conventional constitutive models of soil aviour show very poor predictions. This onstrates the importance of using a model simulates the behaviour of soil over a wide ge of strain increments and with changes in path direction.

WORDS: centrifuge modelling; clays; constitutive ions; ground movements; numerical modelling analysis; stiffness.

La réaction tension/déformation de l'argile préconsolidée dépend à la fois de l'état de l'argile et des charges antérieures, notamment des directions relatives de la charge présente et des charges précédentes. L'exposé décrit un modèle de sol constitutif qui prédit ce comportement en permettant des déformations élasto-plastiques engendrées par deux surfaces cinématiques de durcissement emboîtées dans une surface limite classique d'argile du Cambrien modifiée. Ce modèle relativement simple n'exige que huit paramètres, chacun avec une base rationnelle, et pouvant être déterminés à partir d'un petit nombre d'essais bien contrôlés des parcours de tension. Les prédictions du comportement du sol faites à l'aide de ce modèle sont comparées aux données fournies par des essais triaxiaux des parcours de tension. La bonne corrélation entre les deux ensembles de valeurs confirme que le modèle peut prédire les caractéristiques essentielles du comportement du sol. L'exposé illustre les autres applications possibles de ce modèle à l'analyse géotechnique en comparant les prédictions faites à l'aide du modèle (en conjonction avec une analyse des éléments finis) aux données fournies par une série spéciale d'essais centrifuges d'une fondation circulaire chargée sur de l'argile préconsolidée. On a soigneusement documenté les tensions successives dans les essais pour pouvoir les reproduire dans les analyses. Les calculs ont reproduit les principales caractéristiques du mouvement de sol observé, notamment le profil de surface. Par contraste, les modèles constitutifs classiques du comportement du sol donnent de très mauvaises prédictions. Cela montre qu'il est important d'utiliser un modèle qui simule le comportement du sol sur une vaste gamme de tensions et avec des changements de direction des charges.

INTRODUCTION

ıendent on its most recent loading path or paths kinson *et al.*, 1990). The non-linear stress–ıin response of a wide range of overconsolidated ys has been examined, both for research pur-es and, increasingly, as part of design proce-es in industry.

The importance of improving soil models to take antage of a greater understanding of soil stress–in behaviour has been perceived by many re-rchers. Jardine *et al.* (1986), Jardine *et al.* 91) and Gunn (1993), among others, have devel-d variable modulus models to incorporate non-ar stiffness in finite element analyses and have ıonstrated the importance of this refinement to calculation of ground movements. In addition, ıpson (1992, 1993) developed a model based on ovel analogue of a man dragging bricks, which ulates both non-linearity and the effect of recent ss history, as reported by Richardson (1988). : 'brick' model was shown to produce improved lictions of movements around deep basement avations but the influence of recent stress history . not specifically explored.

The model described in this paper is derived n the elasto-plastic kinematic hardening models ɔosed by Mröz *et al.* (1979), Prevost (1978) Hashiguchi (1985), which can easily be adap-to model the required features of the stress–in response of soils; it was originally developed Stallebrass (1990) and outlined by Atkinson & lebrass (1991), where the use of kinematic lening models are discussed. The model uses simplest possible configuration of kinematic ıces while permitting all the important features he soil behaviour to be replicated.

The principal aim of this paper is to describe in il the new constitutive model and to demon-:e, by simulating triaxial test data and model ;, the advantages offered by using this type of lel for predicting ground movements in over-ɔlidated soils. Data which illustrate the impor-e of recent stress history and non-linearity in ıent tests are briefly reviewed. These data lead he derivation of the constitutive soil model, :h is implemented in the Critical State Program SP) finite element computer program (Britto & n, 1987). Subsequently, the benefits to geotech-l design are investigated by evaluating finite ıent computations of a simple boundary value lem against centrifuge model tests. A key fea-of this work is that a constitutive model has : formulated which describes essential features ɔil stress–strain behaviour evident in carefully rolled triaxial tests, and this model has then

STRESS–STRAIN CHARACTERISTICS OF OVERCONSOLIDATED CLAYS

An overconsolidated soil deposit is created geologically by a combination of, for example, one-dimensional swelling and recompression, which it undergoes to reach its current state. This loading is caused by processes such as erosion of soil during glaciation, redeposition of alluvial deposits and fluctuations in the water table, and defines the stress history of the deposit. There may also be previous construction works which will contribute to the recent stress history. Subsequent construction of a structure, whether it is a retaining wall, tunnel, deep basement or foundation, will cause soil elements around the structure to be loaded such that, in general, the applied stress path constitutes a change in stress path direction. This paper is concerned with the stress–strain response of overconsolidated clays due to such construction, that is, during monotonic loading paths, either drained or undrained, which often follow a distinct change in load path direction. The behaviour of overconsolidated clays has been discussed in detail elsewhere (e.g. Atkinson & Sallfors, 1991; Jardine *et al.*, 1984; Atkinson *et al.*, 1990). The data presented below illustrate the key features of the stress–strain response, which need to be included in a constitutive model. The data are for Speswhite kaolin, which was chosen for its low creep properties. Full details of the experimental procedure used to obtain the test data presented here are given by Stallebrass (1990).

In reviewing the stress–strain response of overconsolidated clay, Atkinson & Sallfors (1991) concluded that all the following factors were influential: the change in stress or strain since the start of loading, the current and previous stress paths, the time spent at a constant stress before loading, the mean effective stress and the overconsolidation ratio. Atkinson *et al.* (1990) used the term 'recent stress history' to describe both the previous stress path and the time spent at a constant stress state before an imposed change in stress. Richardson (1988) investigated these two effects and found that stiffness increased logarithmically with time spent at constant stress, independently of any changes in stress path direction; thus the two effects are additive. Hence the two elements of recent stress history can be dealt with separately. One of the main innovations in the constitutive model that will be described is its ability to simulate the effect of the previous stress path, which is the effect referred to when the term 'recent stress history' is used herein.

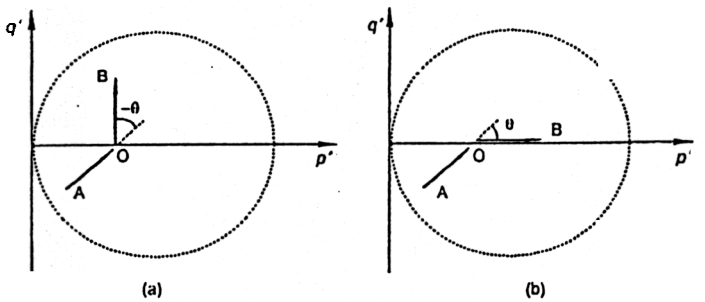

Fig. 1. Typical stress probes showing recent stress history (AO) and (a) constant p' path or (b) constant q' path along which stiffness characteristics are measured

ıditions of axial symmetry was represented by uming that the soil was cross-anisotropic, as icated in equation (1). These conventions will followed in the comparison of test data with dictions in this paper.

$$\begin{bmatrix} \delta\varepsilon_v \\ \delta\varepsilon_s \end{bmatrix} = \begin{bmatrix} \frac{1}{K'_c} & \frac{1}{J'_{2c}} \\ \frac{1}{J'_{1c}} & \frac{1}{3G'_c} \end{bmatrix} \begin{bmatrix} \delta p' \\ \delta q' \end{bmatrix} \qquad (1)$$

e notation G'_c and K'_c has been adopted to tinguish the compliance moduli defined by tinson *et al.* (1990) from the conventional defi- on of G' and K'.

The conclusions drawn from the experimental k reported by Atkinson *et al.* (1990) and exten- by Stallebrass (1990) using test procedures ich could measure strains as low as 0·004% e as follows.

As reported by other authors, the stiffness of a soil loaded along a given stress path decreases non-linearly with change in stress or strain. The stiffness is initially heavily dependent on recent stress history (Fig. 2(a)) such that the stiffness curve is only unique for a fixed recent stress history.

The pattern of strain paths (Fig. 2(b)) shows that the recent stress history of the soil determines whether the initial response of the soil is dilatant or compressive. Stress path rotations of $\theta = 90°$ and $\theta = -90°$ represent either end of the range of the behaviour, and this can also be observed in undrained tests (Fig. 3).

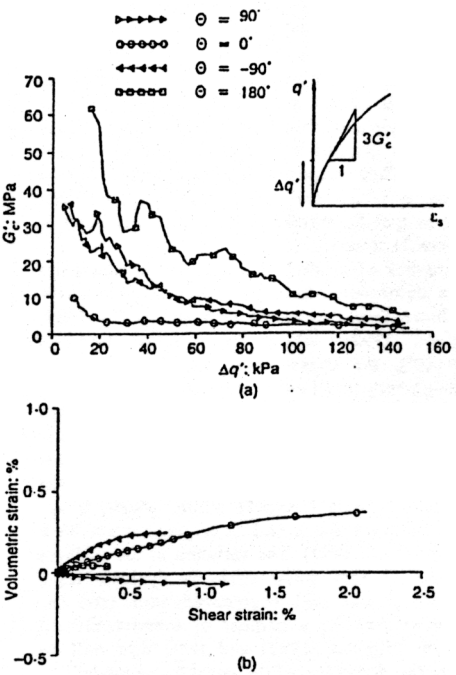

Fig. 2. Data from a test on Speswhite kaolin, constant p' loading, $p'_i = 300$ kPa, $p'_m = 720$ kPa: (a) tangent stiffness data; (b) strain paths

paths in compression and extension or swelling.

(*d*) The strains measured in these tests are not

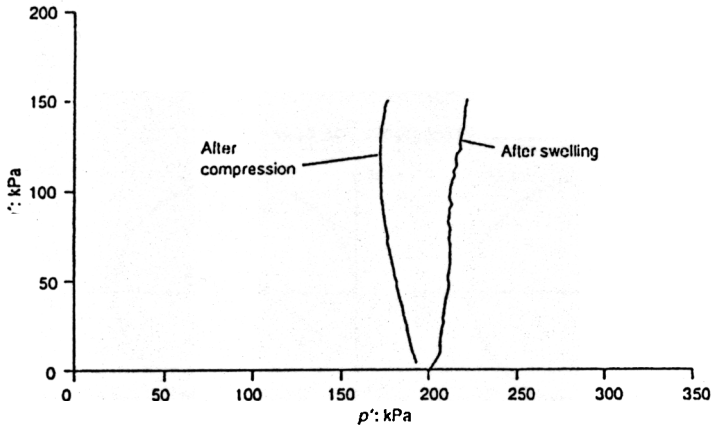

Fig. 3. Undrained effective stress paths for reconstituted samples of London clay, $p'_i = 200$ kPa, $p'_m = 663{\cdot}5$ kPa, after isotropic swelling and recompression

The effect of recent stress history has also been investigated by, for example, Jardine (1985, 1992) and Smith *et al.* (1992), using a different experimental approach. The main result of those investigations was the observation of two zones of behaviour in stress space, which exist within a bounding yield surface and which change shape and size as the soil is subjected to different stress histories. They proposed that these zones defined regions in which the stress–strain response conforms to specific criteria such as linear elasticity or recoverable strains.

A review of existing data on the characteristics of the deformation at strain levels below 0·004% has shown that in dynamic tests (Rampello, 1989; Viggiani, 1992), which apply stress reversals ($\theta = 180°$), the stress–strain response is elastic. Although very small strain static measurements can now be made, as reported by Tatsuoka & Shibuya (1991), it is still not clear whether an elastic threshold strain can always be identified in shear tests on overconsolidated soil and what controls the magnitude of this threshold strain, which, it appears, can vary for a soil at a given stress state (Mukabi *et al.*, 1995). The variation of the stiffness measured at very small strain in dynamic tests, G'_0, with p' and with overconsolidation ratio has been quantified for a number of overconsolidated clays by Viggiani (1992) and these data will be used in the derivation of the constitutive model.

THE CONSTITUTIVE SOIL MODEL

The three-surface kinematic hardening (3-SKH) soil model was formulated specifically to simulate the behaviour of clays at overconsolidated stress states and during early stages of loading. In addition, the model makes use of the framework of critical state soil mechanics (Schofield & Wroth, 1968) and is also valid near failure, giving improved predictions relative to conventional critical state models, such as the Modified Cam-clay model, at heavily overconsolidated stress states for a wide range of changes in stress ratio. As discussed above, it is reasonable to assume that the deformation of overconsolidated soils is elasto-plastic, except possibly after significant changes in stress path direction when at very small subsequent stress or strain changes elastic deformations may occur. Furthermore, the stress–strain response is initially dependent on the recent stress history of the soil, and this effect gradually decreases as loading continues, until the soil loses its memory of the previous loading path.

Incorporating kinematic yield surfaces within a conventional state boundary surface is a straightforward method of representing the memory of recent loading history. Used within the framework of critical state soil mechanics this approach offers the possibility of combining two established theories to formulate a conceptually simple model that nevertheless simulates all the important features of the behaviour of overconsolidated soils.

Al Tabbaa (1987) and Al Tabbaa & Wood (1989) recognized the benefit of kinematic yield surfaces and they developed a 'bubble' model using a single surface within the Modified Cam-clay state boundary surface. The 3-SKH model is an extension of that model, but significantly incorporates an additional kinematic surface, which is essential if both the effect of recent stress history and yield at small strains or changes in stress are

to be simulated, as suggested by Atkinson & Stallebrass (1991).

For simplicity, the model will be described in terms of the triaxial stress and strain invariants p', q', ε_s and ε_v. In order to implement the model in a finite element program it should be formulated in general stress space, and this was carried out by replacing q' by the deviatoric stress tensor s_{ij} (Chan, 1992). An example of this procedure is illustrated in equation (3b). The symbol ':' is the tensorial contraction and the factor 3/2 is introduced because of the definition of q'. In this way the centre of the surface is represented by a tensor with the correct dimension in general stress space. Hence, the general principle that the recent stress history of the soil affects the deformation during loading holds whether the stress paths are in axisymmetric or general stress space. Some very limited data from three-dimensional cube tests reported by Stallebrass (1990) support this principle. Any attempt to model the behaviour in general stress space in more detail would have to be accompanied by more extensive experimental data than currently available.

The model is represented in p'–q' space in Fig. 4, which shows a projection of the Modified Cam-clay state boundary surface above an elastic unload–reload line, referred to as the bounding surface, and two nested kinematic surfaces: the yield surface and the history surface, which are geometrically similar to the bounding surface. The surfaces are defined by the following equations.

Bounding surface

$$(p' - p'_o)^2 + \frac{q'^2}{M^2} = p'^2_o \tag{2}$$

History surface

$$(p' - p'_a)^2 + \frac{(q' - q'_a)^2}{M^2} = T^2 p'^2_o \tag{3a}$$

or, in general stress space,

$$(p' - p'_a)^2 + \frac{3}{2}\frac{(s_{ij} - s^a_{ij}):(s_{ij} - s^a_{ij})}{M^2} = T^2 p'^2_o \tag{3b}$$

Yield surface

$$(p' - p'_b)^2 + \frac{(q' - q'_b)^2}{M^2} = T^2 S^2 p'^2_o \tag{4}$$

In equation (3a), p'_a and q'_a represent the stress state at the centre of the history surface and in equation (4), p'_b and q'_b represent the stress state at

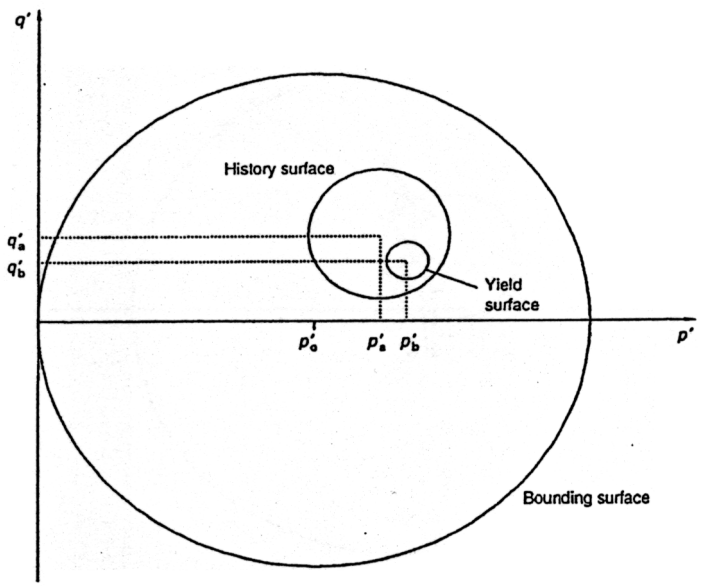

Fig. 4. Sketch of the 3-SKH model in triaxial stress space

the centre of the yield surface. The dimensions of the three surfaces are linked by the two fixed ratios T and S. The product TS defines the ratio of the stress change required before yield to p'_o, and T defines the ratio of the extent of the effect of recent stress history to p'_o.

The kinematic surfaces move when the current stress state lies on one or more surface, one of which must be the yield surface, and the load increment is in the range $\pm 90°$ to the outward normal to the surface(s). The magnitude and direction of the movement of the surfaces is controlled by translation laws of the same form as those used in the 'bubble' model (Al Tabbaa, 1987) and other similar models (Mröz *et al.*, 1979; Hashiguchi, 1985). These laws follow a rule which states that the centre of a surface should always move along a vector joining the current stress state to its conjugate point on the next surface, where the conjugate points are as shown in Fig. 5. This rule ensures that, as the surfaces are dragged by the current stress state, they never intersect and it causes the surfaces to align gradually along the current stress path direction. In the model there is a separate component to the translation rule which governs the translation of a surface in contact with one or more other surfaces. It is the translation rules which allow the model to provide a memory of previous loading history when the loading direction is changed.

If the stress state is within the yield surface, deformations are governed by the isotropic elastic constitutive equation (5), otherwise the stress–strain behaviour is elasto-plastic with associated flow on all surfaces and a hardening rule which extends the standard Modified Cam-clay hardening rule, linking the expansion or contraction of all three surfaces to changes in volumetric strain. When formulated for the yield surface this standard expression is of the form given below in equation (6). In these equations λ^* and κ^* represent the gradient of the normal compression line and the elastic swelling lines in $\ln v - \ln p'$ space and G'_{ec} is the elastic shear modulus, discussed later.

$$\begin{bmatrix} \delta\varepsilon_v^e \\ \delta\varepsilon_s^e \end{bmatrix} = \begin{bmatrix} \kappa^*/p' & 0 \\ 0 & 1/3G'_{ec} \end{bmatrix} \begin{bmatrix} \delta p' \\ \delta q' \end{bmatrix} \tag{5}$$

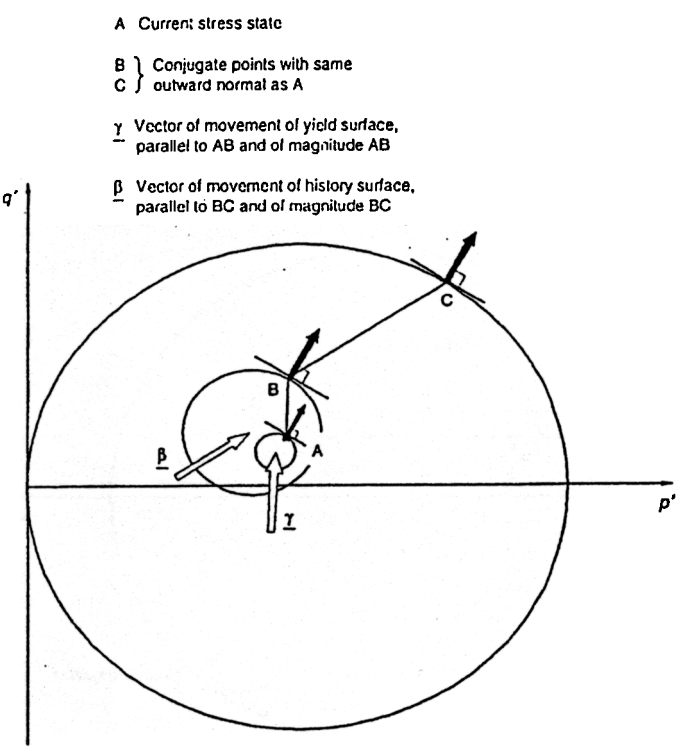

Fig. 5. Sketch illustrating the principle of the translation rule for the kinematic surfaces

$$\begin{bmatrix}\delta\varepsilon_v^p\\ \delta\varepsilon_s^p\end{bmatrix} = \frac{1}{h_o}\begin{bmatrix}(p'-p_b')^2 & (p'-p_b')\dfrac{(q'-q_b')}{M^2}\\ (p'-p_b')\dfrac{(q'-q_b')}{M^2} & \left(\dfrac{(q'-q_b')}{M^2}\right)^2\end{bmatrix} \times \begin{bmatrix}\delta p'\\ \delta q'\end{bmatrix}$$

where

$$h_o = \frac{(p'-p_b')}{\lambda^*-\kappa^*}\left(p'(p'-p_b') + q'\frac{(q'-q_b')}{M^2}\right) \tag{6}$$

Equations (5) and (6) reduce to the Modified Cam-clay constitutive equations when all the surfaces are in contact. However, the hardening modulus h_o, as defined in equation (6) cannot be used without modification as it predicts infinite strains at a number of points on the kinematic surfaces (Al Tabbaa, 1987). Following Al Tabbaa (1987), additional terms are added so that h_o is replaced by $h = h_o + H_1 + H_2$, where H_1 and H_2 are functions of the position of the history and yield surfaces respectively. H_1 is a function of b_1, the scalar product of the outward normal at B and the vector $\underline{\beta}$ (Fig. 5) normalized by its maximum value b_{1max}. Similarly, H_2 is a function of b_2, the scalar product of the outward normal at A and the vector $\underline{\gamma}$ (Fig. 5) normalized by its maximum value b_{2max}. Both b_1 and b_2 become zero when the surfaces are in contact, such that the hardening rule reduces to that for Modified Cam-clay. Equation (7) gives the full expression for the hardening modulus h, which replaces h_o in equation (6). The additional parameters that appear in H_1 and H_2 in equation (7) ensure that there is a smooth change in stiffness when the surfaces are in contact. The exponent in the hardening modulus, ψ, changes the rate of decay of stiffness with stress change.

$$h = \frac{1}{\lambda^*-\kappa^*}\left[(p'-p_b')\left(p'(p'-p_b') + q'\frac{(q'-q_b')}{M^2}\right) + \left(\frac{b_1}{b_{1max}}\right)^{\psi} p_o'^3 S^2 + \left(\frac{b_2}{b_{2max}}\right)^{\psi} p_o'^3\right] \tag{7}$$

The link between the stiffness predicted by the model and the configuration of the surfaces is illustrated in Fig. 6. Figs 6(a) and (b) show the

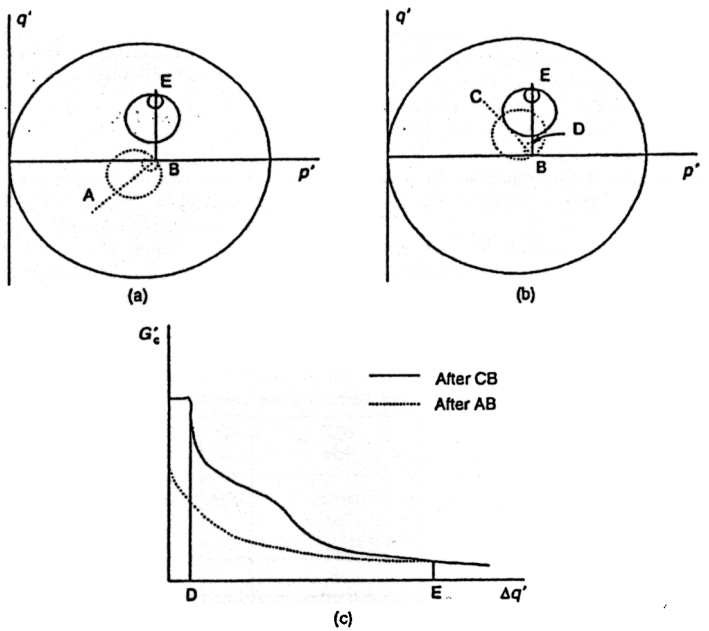

Fig. 6. Diagrammatic representation of the variation of stiffness with recent stress history and loading predicted by the model as the kinematic surfaces translate

configuration of the kinematic surfaces before constant p' shearing along BE, following two different stress paths AB and CB. At B the kinematic surfaces have become aligned with the initial stress path and the position of the surfaces means that the initial stiffness when the soil is sheared after path AB is less than the stiffness for the soil loaded from C to B (Fig. 6(c)), since in the latter case when shearing begins the stress state initially moves across the yield surface so that the deformations are elastic and the stiffness is at a maximum. This higher stiffness corresponds to the path which constitutes the greatest stress path rotation.

Eight soil parameters are required to define the model. Five of these parameters have their origin in the Modified Cam-clay model. The normal compression line is defined in $\ln v - \ln p'$ space, following Butterfield (1979), with a constant slope of λ^* and a specific volume N at $p' = 1$ kPa. The critical state line also has a constant slope λ^* in $\ln v - \ln p'$ space and is further defined in stress space by the coefficient of friction M where $q' = Mp'$. The parameters defining the elastic deformations are κ^* and G'_{ec}. An estimate of the value of κ^* can be obtained by plotting K'_c/p' against p'/p'_m for isotropic swelling from a normally consolidated state and using data at the start of the curve. Similarly, if strain measurements can be made with sufficient accuracy, G'_{ec} may be estimated from the start of constant p' shearing following a complete stress reversal. Alternatively, G'_{ec} can be deduced from dynamic measurements of G'_0, to which it is equivalent for isotropic elastic deformation. In the model G'_{ec} can be assumed to be constant, but in the boundary value analyses presented in this paper G'_{ec} varies with p' and overconsolidation ratio R_o according to the power function proposed by Viggiani (1992), and as given in Table 1.

Figure 7(a) shows a pattern of isotropic stress paths in which one loading stage is repeated for two different stress histories, $\theta = 0°$ and $\theta = 180°$. This enables values for T and S to be estimated from the two sets of stress–strain data plotted as K'_c against $\Delta p'$ in Fig. 7(b). The final parameter, ψ, which is an exponent in the hardening modulus as given in equation (7), is the only parameter which cannot be obtained directly from the experimental data and its value is derived from parametric studies.

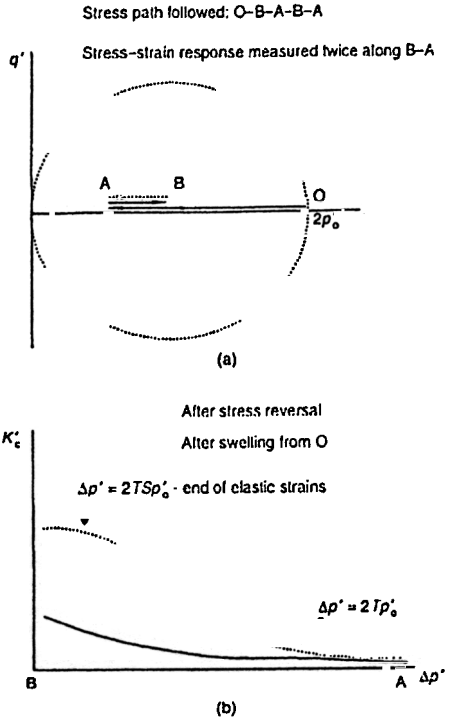

Fig. 7. Sketch showing (a) isotropic stress paths required to determine values for parameters T and S; (b) typical stiffness plots from which T and S can be estimated

Table 1. Soil parameters used in single element and finite element analyses

	M	λ^*	e_{cs}	κ^*	G'_{ec}†: kPa	T	S	ψ	k_v‡: mm/s	k_h‡: mm/s
Three-surface kinematic hardening model (Stallebrass, 1990; Viggiani, 1992)	0·89	0·073	1·994	0·005	60 000 or $1964(p'/p'_r)^{0.65}R_o^{0.2}$	0·25	0·08	2·5	$0{\cdot}47 \times 10^{-6}$	$1{\cdot}37 \times 10^{-6}$
	M	λ	e_{cs}	κ	ν				k_v‡	k_h‡
Modified Cam-clay model (Morrison, 1994)	0·89	0·18	1·97	0·035	0·3				$0{\cdot}47 \times 10^{-6}$	$1{\cdot}37 \times 10^{-6}$

† p'_r is a reference pressure equal to 1 kPa.
‡ Permeability calculated from formulae of Al Tabbaa (1987) using appropriate values of voids ratio.

EVALUATION OF MODEL AGAINST TRIAXIAL TEST DATA

A preliminary evaluation of the model against results from the series of stress path triaxial tests was carried out using a computer program which modelled the tests as a single element. A set of model parameters for Speswhite kaolin was obtained using the procedure outlined above and, except for G'_{ec} which was defined differently in the boundary value analyses, the same set of parameters was used throughout both the comparison with triaxial test data and the analyses of the centrifuge tests which are described later; the parameters are given in Table 1. It is important to note that there has been no attempt to tune the parameters for the particular data presented. Because the parameters are determined rigorously, any differences between observations and predictions simply illustrate potential shortcomings in this relatively simple approach to modelling soil behaviour. A detailed evaluation of the model is given by Stallebrass (1990). The tests were reproduced by following the same stress paths, in the same order. This was necessary because there is a second-order effect on stiffness from the stress paths before the path defining the angle of rotation θ.

Figure 8 shows a comparison between experimental stiffness data from a test on Speswhite kaolin and model predictions. It is clear that the general pattern of the behaviour is well reproduced, although at small changes in stress the experimental data are not sufficiently accurate to allow a detailed comparison to be made. At the start of loading, plots of stiffness data accentuate inaccuracies or errors in the data, whereas at larger changes in stress a stress–strain curve (Fig. 9) provides the most critical comparison. The experimental and predicted unload–reload curves given in Fig. 9 indicate that at this stress state at least, the model overpredicts the reduction in stiffness for larger stress changes. Fig. 10(a) shows a comparison between the pattern of strain paths obtained experimentally and those predicted using the single element simulation. The pattern of the data is correct but in general the predicted volumetric strains are more dilatant than those observed.

All the data given above are at stress states with stress ratios q'/p' less than or equal to 0·6, that is, for Speswhite kaolin reasonably far from failure. Fig. 11, which was produced from single element computations, illustrates the response of the model at stress states near failure on the critical state line. A series of drained loading tests starting at states both wet and dry of critical, but with the same preconsolidation pressure, has been normalized by p'_e, the equivalent mean effective pressure on the normal compression line. The first interesting feature of these data is that none of the stress paths reach the Modified Cam-clay state boundary surface, shown plotted on the figure as a normalized constant volume section, until the point representing the critical state line. (Note that a state boundary surface normalized by p'_e will not be ellip-

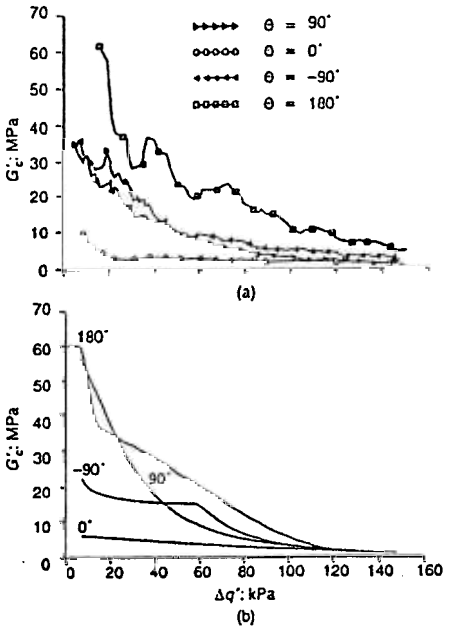

Fig. 8. Comparison between stiffness data computed from a single element simulation and measured data from Fig. 2

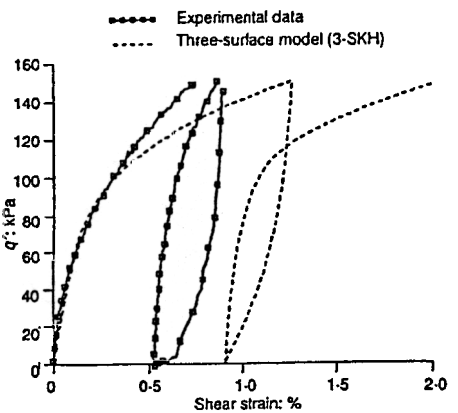

Fig. 9. Cycle of loading during test on Speswhite kaolin, $p'_i = 300$ kPa, $p'_m = 720$ kPa: comparison between predicted and measured stress–strain response

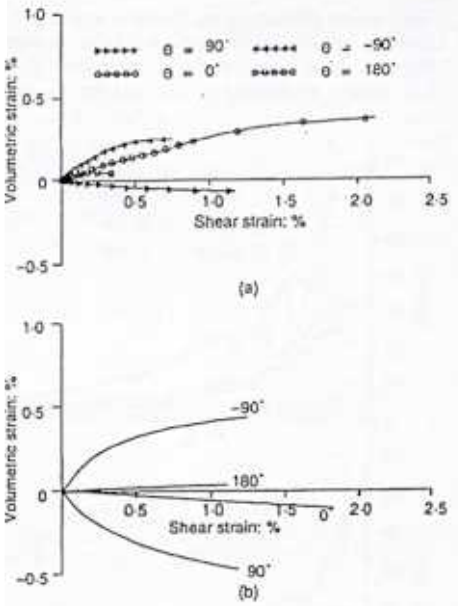

Fig. 10. Comparison between strain paths from (a) test data (shown in Fig. 2); (b) computer simulation

tical, although the low value of κ^* used in the model will, of course, make the surface appear almost elliptical.) The model predicts this behaviour because plastic volumetric strains, either positive or negative depending on the relative position of the stress state and surfaces, occur inside the state boundary surface. Thus the stress state can move to new 'elastic walls', as defined by Schofield & Wroth (1968), and so does not have to reach the state boundary surface before being able to move towards a critical state. Whether the stress state reaches the state boundary surface before it attains a critical state depends on the magnitude of the plastic volumetric strains at states inside the state boundary surface. If these strains are significant, the state boundary surface used in the model cannot be defined by normalizing shear tests. An important advantage of this feature in terms of modelling the behaviour of overconsolidated soils is that on the dry side of critical state the peak states predicted by the model are at much lower stress ratios than those predicted by conventional critical state models such as Modified Cam-clay. An additional characteristic of these computations is that stress paths for shearing under undrained soil conditions are well inside stress paths starting from the same stress state but for drained soil conditions. This is consistent with observations

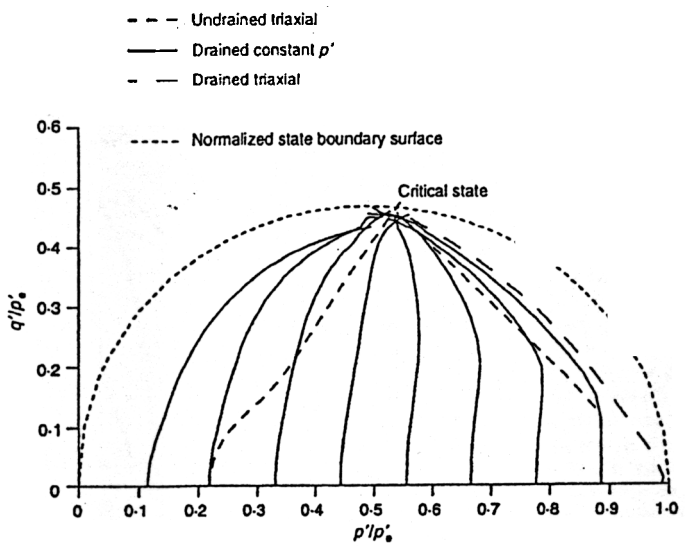

Fig. 11. Normalized stress paths generated by the 3-SKH model

reported by Gens & Potts (1982) for Lower Cromer Till.

CENTRIFUGE MODEL FOUNDATION TESTS

Comparisons with triaxial test data have clearly shown that the 3-SKH model reproduces the main features of the behaviour of overconsolidated soils. They have not shown, however, whether these features of soil behaviour have sufficient effect on the magnitude and distribution of deformations around structures constructed in overconsolidated soils for the use of this type of soil model to be justified in geotechnical design. To carry out a preliminary evaluation of the effectiveness of the model in finite element analyses of boundary value problems, the model predictions were compared with data from real events, in this case centrifuge model tests.

For the purposes of comparison with a new numerical prediction, data from centrifuge model tests are preferred to field data because it is possible to avoid some of the uncertainties in field results such as soil variability, scarcity of instrumentation and the uniqueness of the data. In centrifuge model tests the soil is uniform with well-known properties, stresses, loading and, most importantly here, the stress history is controllable and the model can be well instrumented. In addition, the tests can be tailored to a specific purpose, in this case, to measure the response of overconsolidated soil to loads which result in small changes of stress or strain. The centrifuge model selected was a circular rigid foundation placed on the surface of a layer of overconsolidated soil. The experiment is relatively simple, and accurate measurements of displacement at the soil surface can be obtained in order to characterize the displacement field in the soil as a whole.

The tests were carried out on the Acutronic 661 geotechnical centrifuge at City University. The arrangement of the soil model, foundation, and the various instrumentation used to measure the applied load, the pore pressure profile in the soil and the surface movements are shown in Fig. 12. The sample of Speswhite kaolin was prepared in a consolidometer before the model was assembled and placed on the centrifuge. The maximum vertical stresses σ'_{vmax} applied by the consolidometer for the three tests from which data are presented are given in Table 2. The soil sample was swelled back to a vertical effective stress of either 100 kPa or 200 kPa, before it was removed from the consolidometer. The series of sketches in Fig. 13 show the effective stress and pore pressure distribution at various stages in the preparation and testing of the model which was used for Test 3. In order to calculate these stresses it was assumed that removing the soil sample from the consolidometer created a suction of −100 kPa throughout the soil layer, that is, that no free water entered the soil sample. If free water entered the sample it could swell back to a lower vertical effective stress, which would influence the final horizontal stress distribution in the sample. Table 2 also gives the water level in the models, the diameter of the foundations B and the initial load on the foundation resulting from the weight of the foundation and the loading pin.

After the model was placed on the centrifuge and the required test acceleration level had been reached, in this case nominally 100 g. pore pressures were allowed to come into equilibrium. The water level in the model was controlled using a standpipe connected to the base sand layer and a layer of liquid paraffin on the soil surface prevented pore water evaporation during the test. The foundation was then loaded at a rate of 2·4 kPa/s, under nominally undrained soil conditions, by one or more load cycles. Load–displacement curves for the three tests are presented in Fig. 14; the slight jump in the curves for Tests 1 and 2 at the start of loading was caused by the gravity loading device used. The differences in the load–displacement curves observed can be attributed to the different water levels in the models and the change in diameter of the foundation B, as noted in Table 2. The comparison between numerical predictions and experimental data will be carried out for Test 3 because in this test the initial jump in load was eliminated.

As shown in Fig. 12, the surface settlement measurements were made at different radii and angles around the foundation. A surface settlement profile was obtained by assuming that the model was axisymmetric and two measurements were taken on certain radii as a check. Inaccuracies in the surface settlement measurements were mainly caused by electronic noise affecting the output from the transducers, and the error in the readings corresponded to approximately ±0·005 mm, that is, $10^{-4}B$. The size of the pad at the end of the transducer probe means that the distance from the centre of the foundation to a settlement point represents a range of ±1·5 mm, that is, $0{\cdot}03B$. To demonstrate the reproducibility of the main features of the results, normalized surface settlement profiles from all three tests are given in Fig. 15. The sets of data are all for approximately the same foundation displacement during the undrained loading cycles but may correspond to different load ratios. The main feature of the surface settlement profiles is the significant heave which develops near to the edge of the foundation; the maximum displacement is at approximately $0{\cdot}25B$ and has reduced by at least 90% by $1{\cdot}5B$. There are negligible displacements at a radius of $3{\cdot}5B$, which is well within the model boundary.

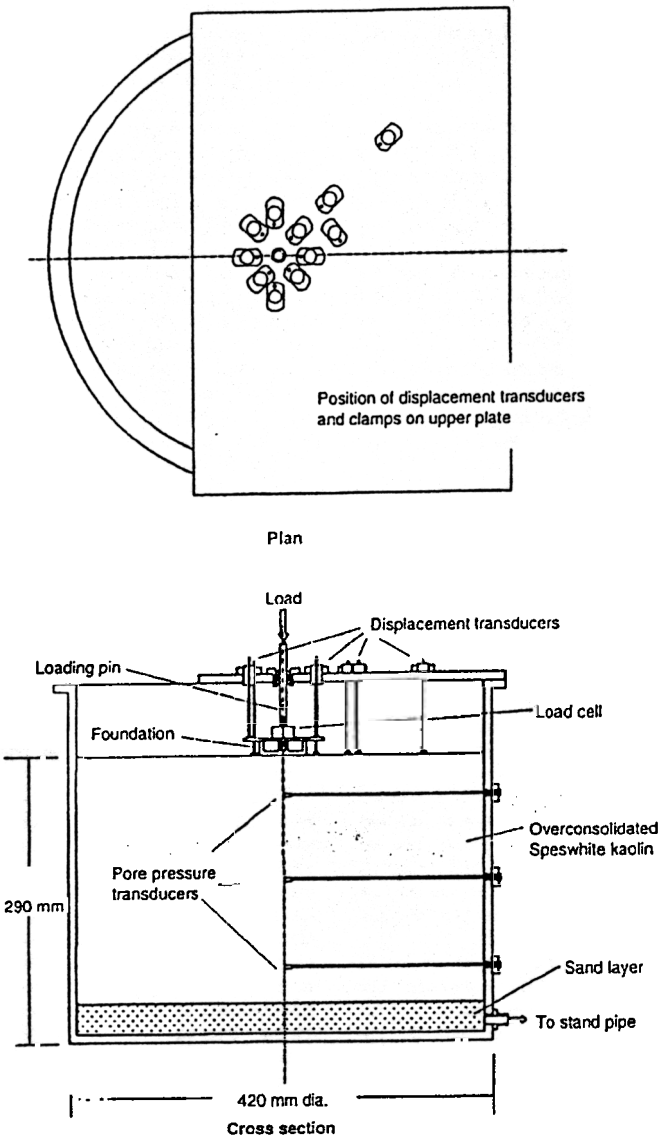

Fig. 12. General layout of centrifuge test

Table 2. Details of centrifuge model tests

Test No.	Foundation diameter B: mm	Stresses reached in consolidometer		Initial load on foundation: N	Water level in model: mm below ground level
		σ'_{vmax}: kPa	σ'_v (final): kPa		
1	50	850	200	214·1	50†
2	50	850	100	226·2	26
3	60	850	100	373·0	52

† Estimated as highest possible water level.

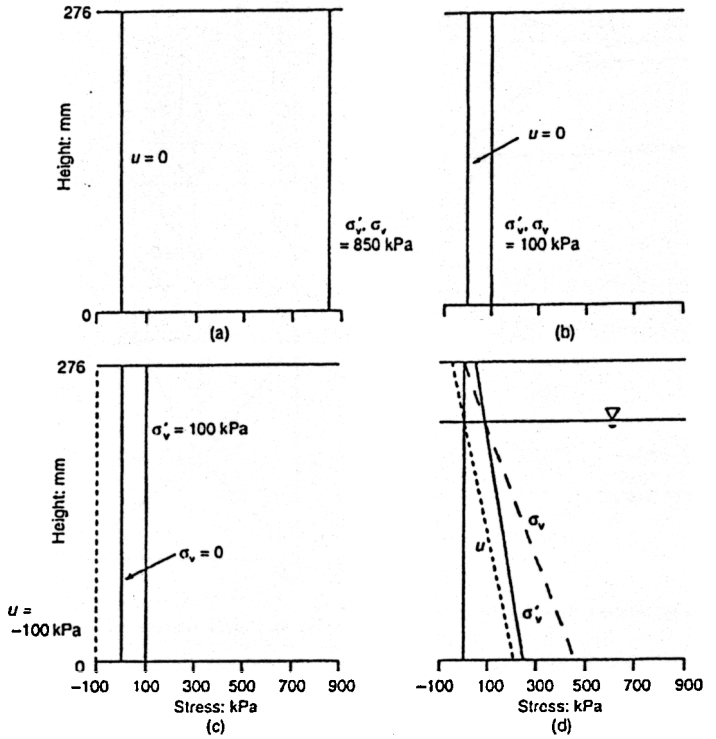

Fig. 13. Change in stress distribution in soil layer during consolidation, preparation and testing of the centrifuge model: (a) maximum stress in consolidometer; (b) end of swelling in consolidometer; (c) during model preparation; (d) in-flight at 95 g after pore pressure equalization.

FINITE ELEMENT ANALYSES OF CENTRIFUGE MODEL TESTS

Two finite element analyses of Test 3 using the version of the CRISP finite element program, modified to incorporate the 3-SKH soil model, are presented: Run 1, in which the soil behaviour was simulated using the new model, and Run 2, in which the conventional Modified Cam-clay model was used. The mesh used to represent Test 3 for both these analyses is given in Fig. 16, which also shows the fixities at the boundaries of the mesh. The CRISP program can model coupled consolidation events and this capability was used in all the analyses. At the start of an analysis employing the 3-SKH model, the kinematic surfaces are centred on the current stress state, so the recent stress history of the soil needs to be recreated to ensure that the surfaces are in the appropriate configuration before loading begins.

The loads applied to the soil in this test can be divided into three main phases:

(*a*) the swelling of the Speswhite kaolin in the consolidometer
(*b*) the equalization of pore pressures on the centrifuge under 100*g* with the foundation and loading pin in place
(*c*) the subsequent loading cycles.

The first two phases represent the recent stress history of the soil before the main loading took place, and in Run 1 both these phases were modelled. To model phase (*a*), a surcharge of 300 kPa was removed from the soil surface over a long time period to simulate the last stages of the swelling of the soil in the consolidometer under essentially drained soil conditions. For phase (*b*), a remaining surcharge of 51·5 kPa was removed, the dead loads applied by the foundation and loading pin were applied by adding a block to the mesh with an appropriate unit weight and the gravitational force on the model was brought to the level attained during the test. Pore pressures generated

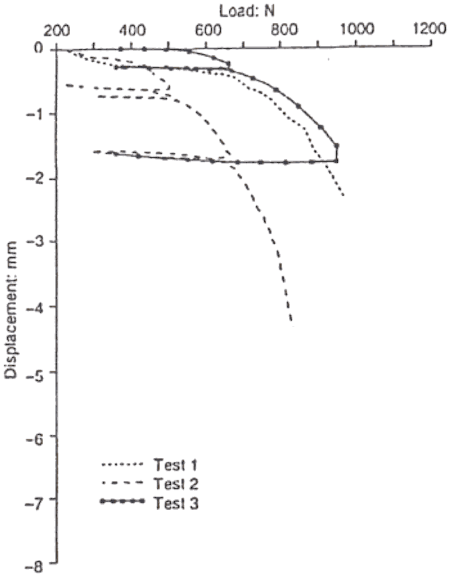

Fig. 14. Load–displacement data for three centrifuge model tests

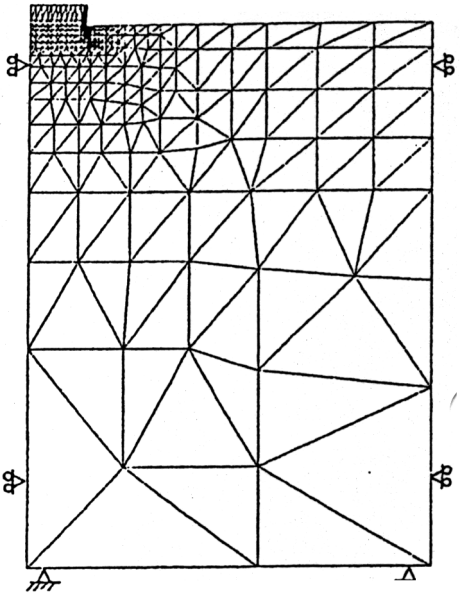

Fig. 16. Finite element mesh for foundation test

by these changes in stress were then allowed to dissipate for the time taken in the experiment. This procedure, developed by Labiouse (1995), enabled the analysis to reproduce exactly the assumed changes in vertical effective stress in the soil in the far field, that is, swelling near the surface and compression near the base of the soil layer, as shown in Fig. 13, as well as an increase in stress under the foundation.

By following these changes in vertical effective stress the model predicts the variation in horizontal stress in the soil layer. As the model soil deforms elasto-plastically at overconsolidated states, a fairly realistic prediction of the horizontal effective stress can be expected. The horizontal effective stresses were not measured during the test and so it was not possible to check the predicted variation of the coefficient of earth pressure K_o. Fig. 17 shows the distribution of K_o both far from and beneath the foundation at the end of the numerical simulation of the recent stress history of the soil, compared with the profile expected from the laboratory investigation by Al Tabbaa (1987) for Speswhite kaolin. The far-field predictions compare well with

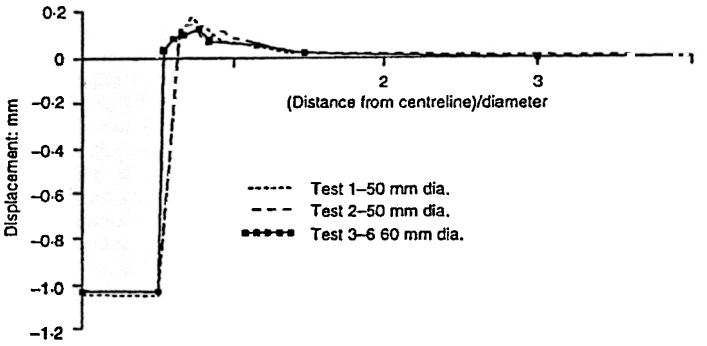

Fig. 15. Settlement profiles for three centrifuge model tests

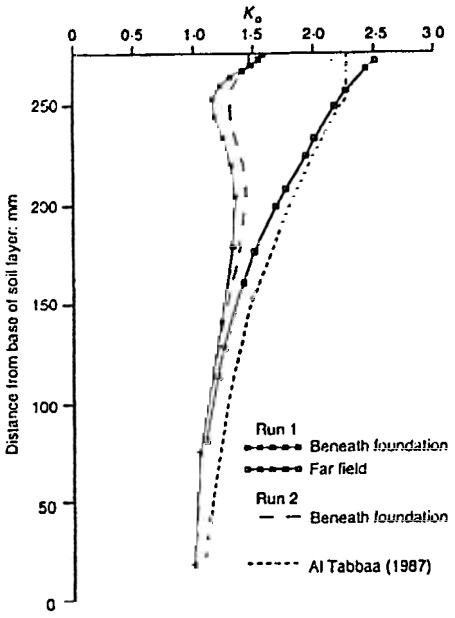

Fig. 17. K_o profiles computed by finite element analyses after simulating recent stress history and before foundation is loaded

the data from Al Tabbaa (1987), except near the soil surface where the predictions exceed the passive failure cut-off at $K_o = 2{\cdot}28$. General formulae proposed by Mayne & Kulhawy (1982) would give K_o values about 30% lower. In Run 2 the far-field K_o profile predicted in Run 1 was the starting point of the analysis and only the dead load provided by the foundation and loading pin were modelled in the initial stage. This was undertaken since simulating the effect of recent stress history using the Modified Cam-clay model is unsatisfactory, as in this case the model soil swells only elastically. The foundation dead load was placed during the analysis merely so that it began at the correct stress state; the K_o profile at the end of this stage is also plotted in Fig. 17.

All the times used for loading and consolidation stages in the analyses were taken directly from the test. Values for the vertical and horizontal permeability of the Speswhite kaolin were obtained from Al Tabbaa (1987) and are given in Table 1, together with the other soil properties used for the two constitutive models. The values of the Modified Cam-clay parameters were obtained by Morrison (1994), who carried out a programme of laboratory tests to derive parameters for a back-analysis of a series of centrifuge tests which also used overconsolidated Speswhite kaolin. The most critical parameter is κ, which was given an average value obtained from a series of unload–reload loops carried out on a sample compressed one-dimensionally to a maximum effective stress of 600 kPa.

The foundation was stiff relative to the soil and assumed to be smooth, owing to the presence of the liquid paraffin at the foundation/clay interface which acted as a lubricant. To enable a smooth interface to be modelled during the final loading stage, the foundation elements were removed at the start of this loading phase and replaced by equivalent nodal forces. Any lateral forces which had developed at the interface during equalization of pore pressures were released and the foundation was then loaded by applying equal displacements across its radius. The rate at which the displacements were applied or removed was controlled to match the rate of increase or decrease of load in Test 3, which was stress controlled.

Data generated by the two finite element analyses are compared with the model test data in Figs 18 and 19. Fig. 18 shows load–displacement relationships for the foundation and Fig. 19 a series of three sets of ground movement profiles taken, first, when the foundation was under a load of 580 N (Fig. 19(a)) and, second, at a load of 660 N (Figs 19(b) and (c)). In all cases it is clear that displace-

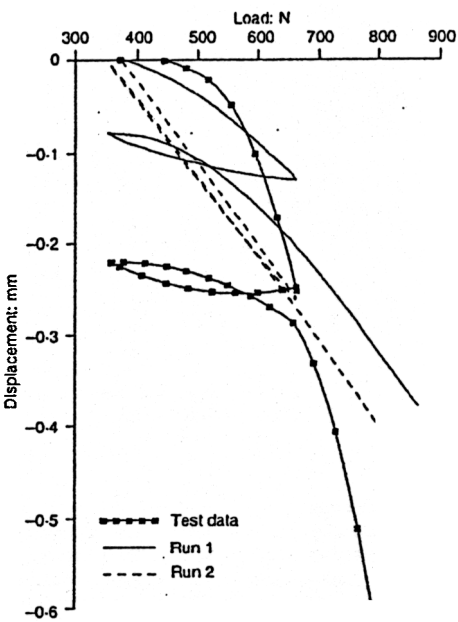

Fig. 18. Comparison between test data and computed load–displacement curves

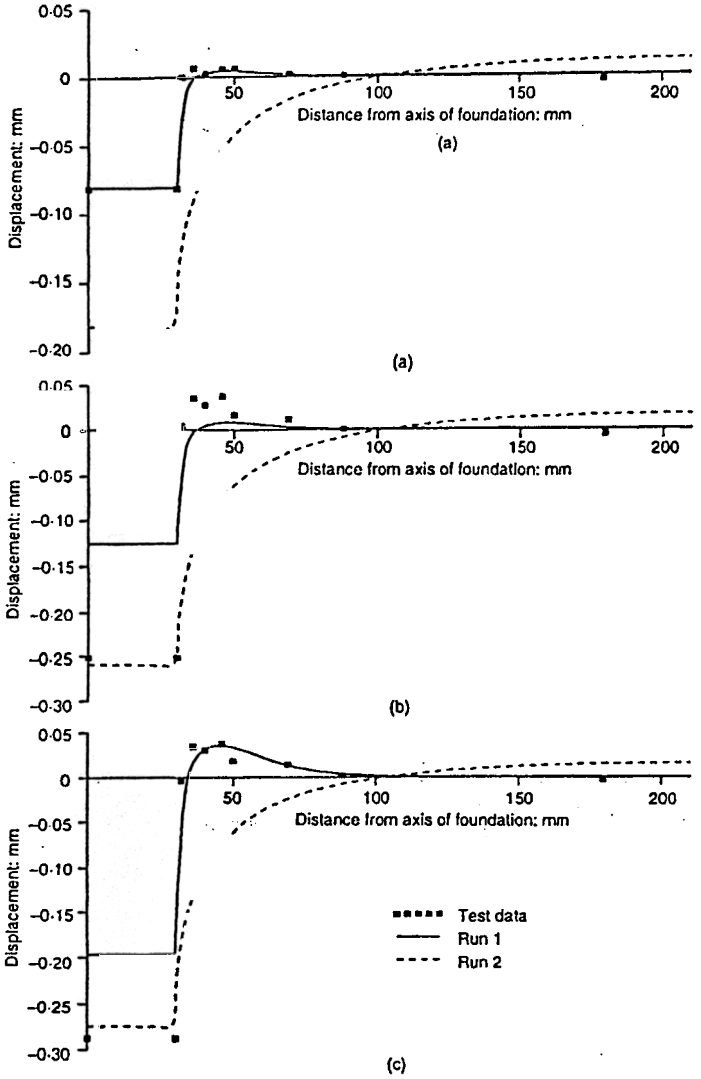

Fig. 19 Comparison between test data and computed settlement profiles at (a) 580 N on first loading; (b) 660 N on first loading; (c) 660 N on reloading

ments calculated from Run 1 are both qualitatively and, generally, quantitatively a better representation of the test data than are the data from Run 2.

The load–displacement response observed in the tests was non-linear with a hysteretic unload–reload cycle, during which there was significant irrecoverable deformation. These characteristics were reproduced qualitatively by predictions from Run 1 but not at all by Run 2, which computed a largely linear load-displacement response with negligible irrecoverable deformation at the end of the unload–reload loop. Both the analyses overpredict the loads at settlements in excess of 0·3 mm, although at this stage the predictions using the new model are less accurate.

A comparison between the test data and the

computed settlement profiles also demonstrates the advantages of the new model. As noted earlier the main characteristics of the settlement profile are a maximum heave at $0{\cdot}25B$ from the foundation and a reduction by more than 90% by $1{\cdot}5B$. Run 1 reproduces these characteristics well and where the computed settlement at the foundation matches the observations (Fig. 19(a)), there is a particularly good correlation with the settlement profile measured in the test. In contrast Run 2 predicts settlement up to a radius of $1{\cdot}5B$ and heave in the far field.

These differences are because, first, the stress–strain relationship used in the new model is non-linear and elasto-plastic, causing localization of deformations. Second, it is possible, using the new model, to model accurately shear-volumetric effects controlling local drainage between areas of high positive excess pore pressures beneath the foundation and negative excess pore pressures near the ground surface adjacent to the foundation. This enables the analysis to predict the magnitude of heave that was observed. In Run 2 the majority of the soil is deforming elastically.

The main discrepancy between the calculations using the new model and the centrifuge data is in the loads predicted at displacements above about 0·3 mm. This may be explained with reference to parametric studies of rigid strip foundations using plane strain finite element analyses incorporating the new soil model (Stallebrass *et al.*, 1995). The analyses showed that a high initial K_0 profile tended to reduce the displacement of the foundation at a given load. As discussed earlier and shown in Fig. 17, there is some evidence that the horizontal stresses predicted by the model are on the high side, particularly near the soil surface, resulting in lower predicted displacements.

For the analyses described, the displacements predicted by the Modified Cam-clay model were governed by the choice of a value for the slope of the elastic swelling line in $\ln v - p'$ space, κ, which governs the elastic response of the soil. For these analyses the value of κ used was that chosen by Morrison (1994). This caused the displacement at the end of the first loading stage to be approximately consistent with the experimental data, but the model was then unable to replicate other features of the load–displacement curve or the displacement field around the foundation.

CONCLUSIONS

Data have been presented that clearly demonstrate the elasto-plastic nature of the stress–strain response of overconsolidated soils, and the importance of recent stress history. Recent stress history affects both the stiffness and the coupled shear-volumetric response of the soil, features which are easily represented using the established family of elasto-plastic soil models incorporating kinematic hardening. The use of two kinematic surfaces is sufficient to model the key features of the observed behaviour.

The new model has been compared against representative stress–strain data from triaxial stress path tests and has been shown to reproduce the main characteristics of these data at small strains. The rigorous approach to this comparison indicated that at larger strains the model may underpredict soil stiffness. It was also noted that at states closer to failure the model can simulate features of soil behaviour observed for Tills, which would otherwise appear not to fit into a conventional critical state soil mechanics framework. This is an important effect of allowing plastic deformation inside the state boundary surface.

Using the new soil model, finite element computations have been made of the distribution of ground movements in the simple boundary value problem of a centrifuge model foundation test. The model test provided a well-controlled event, from which accurate measurements were obtained which were consistent with other test data. The non-linearity of the load–displacement response of the foundation and the distribution of surface movements, that is, heave near the foundation and negligible displacements in the far field, were successfully simulated by the finite element analysis using the new model. The analysis underpredicted the displacement of the foundation as the load increased, which could be due to a difference between the in situ K_0 profile computed in the analyses and the K_0 profile in the centrifuge test. Nevertheless, computations from this analysis represent a substantial improvement on predictions obtained from an equivalent finite element analysis using the Modified Cam-clay model, which is a conventional analysis that might currently be made in engineering practice. In the latter form of analysis it is only possible to choose elastic parameters to obtain the correct displacement at, for example, a single load.

The detailed simulation of the centrifuge test has shown that significant improvements in the prediction of ground movements are possible when using a constitutive model that incorporates sufficient rationally defined flexibility to simulate all the features of the stress–strain response of unstructured overconsolidated soil, including the effect of recent stress history. Key advantages of the 3-SKH model are its conceptual simplicity and the small number of additional parameters that are required to define it. The introduction of plastic deformation controlled by kinematic surfaces inside the state boundary surface has the added benefit of allowing reinterpretation of test data for overconsolidated soils at states near failure.

ACKNOWLEDGEMENTS

The majority of the work described in this paper was carried out while the first author held an SERC-CASE research studentship in collaboration with Ove Arup and Partners, followed by an SERC Postdoctoral Fellowship.

NOTATION

B diameter of the model foundation
b_1 scalar measure of the degree of approach of the history surface to the bounding surface
b_{1max} maximum value of b_1
b_2 scalar measure of the degree of approach of the yield surface to the history surface
b_{2max} maximum value of b_2
e_{cs} void ratio of isotropically normally compressed soil when $p' = 1$ kPa
G'_o shear modulus measured at small strains when the behaviour of the soil is elastic
G'_c shear modulus defined as a compliance as in equation (1)
G'_{cc} elastic shear modulus used in the three-surface kinematic hardening model
H_1, H_2 hardening functions
h_o hardening function when the current stress state lies on the bounding surface
J'_{ic}, J'_{2c} moduli coupling shear and volumetric strains as defined in equation (1)
K_o coefficient of lateral earth pressure at rest
K'_c bulk modulus defined as a compliance as in equation (1)
k_h, k_v coefficients of horizontal and vertical permeability
N specific volume of isotropically normally compressed soil when $p' = 1$ kPa
p' mean effective pressure
$2p'_o$ p' at the intersection of the current swelling line with the normal compression line
p'_a mean effective pressure at the centre of the history surface
p'_b mean effective pressure at the centre of the yield surface
p'_e equivalent pressure: value of p' at the point on the normal compression line at the same specific volume
p'_i value of p' at start of stress probe
p'_m the maximum p' to which the soil has been loaded
p'_r reference value of $p' = 1$ kPa
q' deviatoric stress
q'_a deviatoric stress at the centre of the history surface
q'_b deviatoric stress at the centre of the yield surface
R_o a measure of overconsolidation ratio, defined as $p'/2p'_o$ (Viggiani, 1992)
S ratio of the size of the yield surface to the history surface
s_{ij}, s^a_{ij} deviatoric stress tensor, deviatoric stress tensor at centre of history surface
T ratio of the size of the history surface to the bounding surface
x, y, z Cartesian coordinate axes
$\underline{\beta}$ vector joining the conjugate points on the history and bounding surfaces
$\underline{\gamma}$ vector joining the conjugate points on the yield and history surfaces
ε^e_s, ε^e_v elastic shear and volumetric strain
ε^p_s, ε^p_v plastic shear and volumetric strain
θ angle of stress path rotation
$-\kappa$ gradient of an elastic swelling line in $v-\ln p'$ space
$-\kappa^*$ gradient of an elastic swelling line in $\ln v-\ln p'$ space
$-\lambda$ gradient of the normal compression line in $v-\ln p'$ space
$-\lambda^*$ gradient of the normal compression line in $\ln v-\ln p'$ space
M critical state friction coefficient
ν Poisson's ratio
σ' effective stress
σ'_{vmax} maximum vertical effective stress
τ shear stress
ψ exponent in the hardening modulus

REFERENCES

Al Tabbaa, A. (1987). *Permeability and stress–strain response of Speswhite kaolin*. PhD thesis, University of Cambridge.

Al Tabbaa, A. & Wood, D. M. (1989). An experimentally based 'bubble' model for clay. In *Numerical models in geomechanics* (eds S. Pietruszczak and G. N. Pande), *Proc. 3rd Int. Conf. on Numerical Methods in Geomechanics*, pp. 91–99.

Atkinson, J. H., Richardson, D. & Stallebrass, S. E. (1990). Effect of recent stress history on the stiffness of overconsolidated soil. *Géotechnique* 40, No. 4, 531–540.

Atkinson, J. H. & Sallfors, G. (1991). Experimental determination of stress–strain–time characteristics in laboratory and in situ tests. *Proc. 10th Eur. Conf. on Soil Mech. and Found. Engng, Florence* 3, 915–956.

Atkinson, J. H. & Stallebrass, S. E. (1991). A model for recent stress history and non-linearity in the stress–strain behaviour of overconsolidated soil. *Proc. 7th Int. Conf. on Computer Methods and Advances in Geomechanics, Cairns* 1 555–560.

Britto, A. M. & Gunn, M. J. (1987). *Critical state soil mechanics via finite elements*. Chichester: Ellis Horwood.

Butterfield, R. (1979). A natural compression law for soils. *Géotechnique* 29, No. 4, 469–480.

Chan, A. H. C. (1992). Personal communication.

Gens, A. & Potts, D. M. (1982). A theoretical model for describing the behaviour of soils not obeying Rendulics principle. *Proc. Int. Symp. on Numerical Models in Geomechanics, Zurich* (eds R. Dungar, G. N. Pande and J. R. Studer), pp. 24–32. Rotterdam: Balkema.

Gunn, M. J. (1993). The prediction of surface settlement profiles due to tunnelling. In *Predictive soil mechanics, Proc. Wroth Memorial Symp., Oxford* (eds G. T. Houlsby and A. N. Schofield) pp. 304–316. London: Thomas Telford.

Hashiguchi, K. (1985). Two- and three-surface models of plasticity. *Proc. 5th Int. Conf. on Numerical Methods in Geomechanics, Nagoya*, pp. 125–134.

Jardine, R. J. (1985). *Investigations of pile-soil behaviour with special reference to the foundations of offshore structures*. PhD thesis, University of London.

Jardine, R. J. (1992). Some observations on the kinematic nature of soil stiffness. *Soils Fdns, Japan. Soc. Soil Mech. and Fdn Engng.* **32**, No. 2, 111–124.

Jardine, R. J., Potts, D. M., Fourie, A. B. & Burland, J. B. (1986). Studies of the influence of non-linear stress–strain characteristics in soil-structure interaction. *Géotechnique* **36**, No. 2, 377–396.

Jardine, R. J., St John, H. D., Hight, D. W. & Potts, D. M. (1991). Some practical applications of a non-linear ground model. *Proc. 10th Eur. Conf. on Soil Mech. and Found. Engng. Florence* **1**, 223–228.

Jardine, R. J., Symes, M. J. & Burland, J. B. (1984). The measurement of soil stiffness in the triaxial apparatus. *Géotechnique* **34**, No. 3, 323–340.

Labiouse, V. (1995). Personal communication.

Mayne, P. W. and Kulhawy, F. H. (1982) K_o–OCR relationships in soil. *J. Geotech. Engng, ASCE* **108**, GT6, 851–872.

Morrison, P. R. J. (1994). *Performance of foundations in a rising groundwater environment*. PhD thesis, City University.

Mröz, Z., Norris, V. A. & Zienkiewicz, O. C. (1979). Application of an anisotropic hardening model in the analysis of elasto-plastic deformation of soils. *Géotechnique* **29**, No. 1, 1–34.

Mukabi, J. N., Tatsuoka, F., Kohata, Y., Tsuchida, T. & Akino, N. (1995). Small strain stiffness of Pleistocene clays in triaxial compression. *Proc. Int. Symp. on Prefailure Deformation Characteristics of Geomaterials, Hokkaido* **1**, 189–197.

Prevost, J.-H. (1978). Plasticity theory for soil stress–strain behaviour. *J. Engng Mater. Div., ASCE* **104**, 1177–1194.

Rampello, S. (1989). *Effeti del rigonfiamento sul comportamento meccanico di argille fortemento sovraconsolidate*. PhD thesis, University of Rome.

Richardson, D. (1988). *Investigations of threshold effects in soil deformations*. PhD thesis, City University.

Schofield, A. N. & Wroth, C. P. (1968). *Critical state soil mechanics*. London: McGraw-Hill.

Simpson, B. (1992). 32nd Rankine Lecture. Retaining structures—displacement and design. *Géotechnique* **42**, No. 4, 539–576.

Simpson, B. (1993). Development and application of a new soil model for prediction of ground movements. In *Predictive soil mechanics, Proc. Wroth Memorial Symp., Oxford* (eds G. T. Houlsby and A. N. Schofield), pp. 628–643. London: Thomas Telford.

Smith, P. R., Jardine, R. J. & Hight, D. W. (1992). The yielding of Bothkennar clay. *Géotechnique* **42**, No. 2, 257–274.

Stallebrass, S. E. (1990). *The effect of recent stress history on the deformation of overconsolidated soils*. PhD thesis, City University.

Stallebrass, S. E., Jovicic, V. & Atkinson, J. H. (1995). Influence of geological history on foundation behaviour. *Proc. 11th Eur. Conf. on Soil Mech. and Found. Engng. Copenhagen* **1**, 265–273.

Tatsuoka, F. & Shibuya, S. (1991). Deformation characteristics of soils and rocks from field and laboratory tests. Keynote lecture, *9th Asian Conf. on Soil Mech. and Found. Engng, Bangkok* **2**, 101–170.

Viggiani, G. (1992) *Small strain shear stiffness of fine grained soils*. PhD thesis, City University.